

Anisotropic Diffusion Stencils: From Simple Derivations over Stability Estimates to ResNet Implementations ^{*}

Karl Schrader, Joachim Weickert, and Michael Krause

Mathematical Image Analysis Group, Faculty of Mathematics and Computer Science,
Campus E1.7, Saarland University, 66041 Saarbrücken, Germany
{schrader,weickert,krause}@mia.uni-saarland.de

Abstract. Anisotropic diffusion processes with a diffusion tensor are important in image analysis, physics, and engineering. However, their numerical approximation has a strong impact on dissipative artefacts and deviations from rotation invariance. In this work, we study a large family of finite difference discretisations on a 3×3 stencil. We derive it by splitting 2-D anisotropic diffusion into four 1-D diffusions. The resulting stencil class involves one free parameter and covers a wide range of existing discretisations. It comprises the full stencil family of Weickert et al. (2013) and shows that their two parameters contain redundancy. Furthermore, we establish a bound on the spectral norm of the matrix corresponding to the stencil. This gives time step size limits that guarantee stability of an explicit scheme in the Euclidean norm. Our directional splitting also allows a very natural translation of the explicit scheme into ResNet blocks. Employing neural network libraries enables simple and highly efficient parallel implementations on GPUs.

1 Introduction

Anisotropic diffusion models with a diffusion tensor have numerous applications in physics and engineering. Moreover, they also play a fundamental role in image analysis [11], where they are used for denoising, enhancement, scale-space analysis, and various interpolation tasks such as inpainting and superresolution. Sophisticated nonlinear models with appropriate directional behaviour can close interrupted structures and maintain or create sharp edges. However, to achieve results with only few dissipative artefacts and good rotation invariance, appropriate numerical approximations are needed. They should also come with provable stability guarantees and lead in a natural way to efficient implementations. Ideally they should also exploit the impressive parallelisation potential of modern GPUs. The goal of our contribution is to address these numerical issues.

^{*} This work has received funding from the European Research Council (ERC) under the European Union's Horizon 2020 research and innovation programme (grant agreement no. 741215, ERC Advanced Grant INCOVID).

Our Contributions. Motivated by image analysis applications, where one has a regular pixel grid and aims at simple numerical algorithms, we consider finite difference approximations on a 3×3 stencil. However, our results are also useful for anisotropic diffusion problems in other areas. Our contributions are threefold:

First, we study space discretisations of a general anisotropic diffusion operator on a 3×3 stencil. They split the 2-D anisotropic process into four 1-D diffusions. This class has one free parameter that can be used for quality optimisation. It covers the two-parameter stencil family of Weickert et al. [13], while removing its parameter redundancy and offering a simpler derivation. Moreover, it subsumes many previous discretisations with second-order consistency.

Our second contribution consists of a detailed stability analysis, where we establish fairly tight bounds on the spectral norm of the matrix associated with the stencil family. It allows to derive time step size restrictions for the corresponding explicit scheme (and accelerations that rely on it).

Last but not least, our stencil derivation based on a directional splitting enables the translation of the explicit anisotropic diffusion scheme into a ResNet block [4], which is a highly popular component of neural networks. This showcases that ideas are often shared between numerical schemes and neural architectures. More importantly, it allows simple and fast parallel implementations of anisotropic diffusion on GPUs using neural network libraries such as PyTorch.

Related Work. Many finite difference discretisations for anisotropic diffusion processes exist in the literature. Often they use spatial discretisations on a 3×3 stencil with consistency order two. The stencil class of Weickert et al. [13] comprises seven of them. Our findings offer a simpler derivation and representation of this family. Moreover, we extend the results from [13] by establishing concrete time step size limits for explicit schemes, connecting these algorithms to neural networks, and exploring simple and efficient parallelisations.

Our stencil family originates from a splitting 2-D anisotropic diffusion into four 1-D diffusions along fixed directions. Earlier splittings of this type intended to derive discretisations that are stable in the maximum norm [11,6]. In general this is only possible for fairly mild anisotropies [11]. We consider stencils that offer stability in the Euclidean norm for all anisotropies.

Recent works [1,2,8,9] connect explicit schemes for partial differential equations (PDEs) to the ResNet [4] architecture. For example, Alt et al. [1] show that evolutions of discretised 1-D diffusion models with a scalar-valued diffusivity can be represented as ResNet blocks. In [2], they also explore the 2-D anisotropic case. However, their methodology is limited to evolution equations that arise as gradient descent of an energy functional. This excludes popular methods like edge-enhancing diffusion [11], for which Welk [14] has shown that no energy functional exists. We can translate these methods as well.

Organisation of the Paper. In Section 2, we derive a class of finite difference discretisations on a 3×3 stencil. We establish stability results for the corresponding explicit scheme in Section 3. The fourth section shows how our splitting into 1-D diffusions leads to a translation of this scheme to a ResNet architecture, and it analyses its performance on a GPU. We conclude our paper in Section 5.

2 Discretising Anisotropic Diffusion with the δ -Stencil

In this section, we study a simple and fairly general approach for a space discretisation of anisotropic diffusion on a 3×3 stencil. It is based on a directional splitting into four 1-D diffusion processes, which we discuss first.

1-D Diffusion. To denoise a 1-D signal $f(x) : [a, b] \rightarrow \mathbb{R}$, one can create simplified versions $\{u(x, t) \mid t \geq 0\}$ of it with the nonlinear diffusion process [7]

$$\partial_t u = \partial_x \left(g((\partial_x u)^2) \partial_x u \right) \quad (t > 0), \quad (1)$$

$$u(x, 0) = f(x). \quad (2)$$

Larger diffusion times t correspond to more pronounced simplifications. The diffusivity $g : \mathbb{R} \rightarrow (0, 1]$ is a function that decreases in its argument $(\partial_x u)^2$ in order to preserve discontinuities. At the domain boundaries a and b , we impose reflecting boundary conditions. To prepare for the later translation to a neural architecture, we introduce the flux function $\Phi(\partial_x u) = g((\partial_x u)^2) \partial_x u$. It leads to the evolution equation $\partial_t u = \partial_x(\Phi(\partial_x u))$.

A finite difference discretisation of this 1-D process serves as building block for discretising anisotropic diffusion. To obtain a discrete signal $\mathbf{u} = (u_i) \in \mathbb{R}^N$, we sample u with grid size h . We discretise the derivatives with a forward difference in time and for the inner spatial derivative, and a backward difference for the outer one. This leads to the explicit scheme

$$\frac{u_i^{k+1} - u_i^k}{\tau} = \frac{1}{h} \left(\Phi \left(\frac{u_{i+1}^k - u_i^k}{h} \right) - \Phi \left(\frac{u_i^k - u_{i-1}^k}{h} \right) \right), \quad (3)$$

where $\tau > 0$ is the time step size, i denotes the location, and k the time level.

Anisotropic Diffusion. In image analysis, anisotropic diffusion with a diffusion tensor [11] creates filtered versions $u(\mathbf{x}, t)$ of a scalar-valued (i.e. greyscale) image $f(\mathbf{x})$ by evolving it with the PDE

$$\partial_t u = \mathbf{div}(\mathbf{D} \nabla u), \quad \mathbf{D} = \begin{pmatrix} a & b \\ b & c \end{pmatrix} \quad (4)$$

where we initialise $u(\mathbf{x}, 0)$ with $f(\mathbf{x})$ and use reflecting boundary conditions. The diffusion tensor $\mathbf{D} \in \mathbb{R}^{2 \times 2}$ is symmetric, positive semidefinite with at least one positive eigenvalue. \mathbf{D} may depend on Gaussian-smoothed first order derivatives of the evolving image u . This allows to enhance edges and coherent flow-like structures by smoothing along them, but not perpendicular to them [11].

The δ -Stencil. The discrete setting considers images $\mathbf{f}, \mathbf{u}^k \in \mathbb{R}^N$ obtained by sampling f and $u(\cdot, k\tau)$ with a grid size of h and arranging the pixel values into column vectors. The key idea of our discretisation is the decomposition of an anisotropic 2-D diffusion process into a sum of four nonlinear 1-D diffusions along the axial and diagonal directions

$$\mathbf{e}_0 = \begin{pmatrix} 1 \\ 0 \end{pmatrix}, \quad \mathbf{e}_1 = \frac{1}{\sqrt{2}} \begin{pmatrix} 1 \\ 1 \end{pmatrix}, \quad \mathbf{e}_2 = \begin{pmatrix} 0 \\ 1 \end{pmatrix}, \quad \mathbf{e}_3 = \frac{1}{\sqrt{2}} \begin{pmatrix} -1 \\ 1 \end{pmatrix}. \quad (5)$$

We determine directional diffusivities w_0, \dots, w_3 for the corresponding directions by solving the system of three equations with four unknowns arising from

$$\mathbf{div} \left(\begin{pmatrix} a & b \\ b & c \end{pmatrix} \nabla u \right) \stackrel{!}{=} \sum_{i=0}^3 \partial_{\mathbf{e}_i} (w_i \partial_{\mathbf{e}_i} u). \quad (6)$$

Its solution has one free parameter which we call δ :

$$w_0 = a - \delta, \quad w_1 = \delta + b, \quad w_2 = c - \delta, \quad w_3 = \delta - b. \quad (7)$$

All four 1-D diffusion processes can be discretised as before in (3). Each direction uses three pixels of its 3×3 neighbourhood. Discretising e.g. $\partial_{\mathbf{e}_1} (w_1 \partial_{\mathbf{e}_1} u)$ in the pixels $(i-1, j-1)$, (i, j) , and $(i+1, j+1)$ at distance $h\sqrt{2}$ gives

$$\frac{1}{h\sqrt{2}} \left((\delta + b)_{i+\frac{1}{2}, j+\frac{1}{2}} \frac{u_{i+1, j+1} - u_{i, j}}{h\sqrt{2}} - (\delta + b)_{i-\frac{1}{2}, j-\frac{1}{2}} \frac{u_{i, j} - u_{i-1, j-1}}{h\sqrt{2}} \right). \quad (8)$$

Incorporating all four directions yields the following δ -stencil for $\mathbf{div} (\mathbf{D} \nabla u)$:

$\frac{1}{2} (\delta - b)_{i-\frac{1}{2}, j+\frac{1}{2}}$	$(c - \delta)_{i, j+\frac{1}{2}}$	$\frac{1}{2} (\delta + b)_{i+\frac{1}{2}, j+\frac{1}{2}}$	(9)
$\frac{1}{h^2} \cdot (a - \delta)_{i-\frac{1}{2}, j}$	$\begin{aligned} & - (a - \delta)_{i+\frac{1}{2}, j} - (a - \delta)_{i-\frac{1}{2}, j} \\ & - \frac{1}{2} (\delta + b)_{i+\frac{1}{2}, j+\frac{1}{2}} - \frac{1}{2} (\delta + b)_{i-\frac{1}{2}, j-\frac{1}{2}} \\ & - (c - \delta)_{i, j+\frac{1}{2}} - (c - \delta)_{i, j-\frac{1}{2}} \\ & - \frac{1}{2} (\delta - b)_{i-\frac{1}{2}, j+\frac{1}{2}} - \frac{1}{2} (\delta - b)_{i+\frac{1}{2}, j-\frac{1}{2}} \end{aligned}$	$(a - \delta)_{i+\frac{1}{2}, j}$	
$\frac{1}{2} (\delta + b)_{i-\frac{1}{2}, j-\frac{1}{2}}$	$(c - \delta)_{i, j-\frac{1}{2}}$	$\frac{1}{2} (\delta - b)_{i+\frac{1}{2}, j-\frac{1}{2}}$	

where the x -axis points to the right, and the y -axis to the top. We assume that the diffusion tensor \mathbf{D} is available in the staggered grid locations $(i \pm \frac{1}{2}, j \pm \frac{1}{2})$. This is fairly natural if it relies on first-order derivatives, which can be computed with central differences in a 2×2 neighbourhood [13]. We obtain values in $(i \pm \frac{1}{2}, j)$ and $(i, j \pm \frac{1}{2})$ by averaging:

$$(a - \delta)_{i \pm \frac{1}{2}, j} = \frac{1}{2} \left((a - \delta)_{i \pm \frac{1}{2}, j+\frac{1}{2}} + (a - \delta)_{i \pm \frac{1}{2}, j-\frac{1}{2}} \right) \quad (10)$$

and similar for $(c - \delta)_{i, j \pm \frac{1}{2}}$. Then the δ -stencil family has consistency order two.

Incorporation of the Stencil Family of Weickert et al. [13]. With (10) and $\delta = \alpha a + \beta b + \alpha c$, the δ -stencil family comprises that of Weickert et al. [13] that uses two parameters α and β . This shows that the parameters of the latter contain redundancy which we remove with the δ -stencil. Moreover, our stencil derivation is simpler than the one in [13] that has been obtained by discrete energy minimisation. In [13] it is shown that these stencils comprise seven discretisations from the literature. Since we are not aware of any second-order accurate discretisations on a 3×3 stencil that is not covered by this class, the δ -stencil family may even be more general.

3 Stability Theory for the δ -Stencil

Let the matrix $\mathbf{A} = \mathbf{A}(\mathbf{u}^k)$ act on an image \mathbf{u}^k locally by applying the space-variant δ -stencil. Weickert et al. [13] have already established that \mathbf{A} is negative semidefinite for $\alpha \leq \frac{1}{2}$ and $|\beta| \leq 1 - 2\alpha$. They have also replaced β by a parameter γ such that $\beta = \gamma(1 - 2\alpha) \operatorname{sgn}(b)$ and $|\gamma| \leq 1$. Choosing α close to $\frac{1}{2}$ and γ close to 1 improves rotation invariance and reduces dissipativity in experiments [13]. In practice, parameters $\alpha < 0$ are irrelevant and make a stability analysis more complicated. Thus, we exclude them from now on.

Consider an explicit anisotropic diffusion scheme $\mathbf{u}^{k+1} = (\mathbf{I} + \tau \mathbf{A}(\mathbf{u}^k)) \mathbf{u}^k$ with unit matrix \mathbf{I} , time step size $\tau > 0$, and a negative semidefinite matrix \mathbf{A} with spectral norm $\rho(\mathbf{A}) > 0$. Then stability in the Euclidean norm in terms of $\|\mathbf{u}^{k+1}\|_2 \leq \|\mathbf{u}^k\|_2$ holds if

$$\tau \leq \frac{2}{\rho(\mathbf{A})}. \quad (11)$$

We can bound $\rho(\mathbf{A})$ as follows:

Theorem 1 (Bound on Spectral Norm). *Let the eigenvalues of \mathbf{D} be given by $\lambda_1 \geq \lambda_2 \geq 0$. Assume that $\delta = \alpha(a+c) + \beta b$ where $\beta = \gamma(1 - 2\alpha) \operatorname{sgn}(b)$ for $\alpha \in [0, \frac{1}{2}]$ and $|\gamma| \leq 1$. Then the spectral norm of the matrix \mathbf{A} satisfies*

$$\rho(\mathbf{A}) \leq \frac{4(1-\alpha)(\lambda_1 + \lambda_2) + 2(1-\gamma(1-2\alpha))(\lambda_1 - \lambda_2)}{h^2}. \quad (12)$$

Proof. For the considered choice of α and β , we know from [13] that the symmetric matrix \mathbf{A} is negative semidefinite. Thus, its spectral norm is determined by its smallest eigenvalue λ_{\min} as $\rho(\mathbf{A}) = -\lambda_{\min}(\mathbf{A})$. Let us now bound $\lambda_{\min}(\mathbf{A})$ with Gershgorin's circle theorem [15]. As \mathbf{A} applies the δ -stencil, this theorem states that the smallest eigenvalue of \mathbf{A} is bounded from below by the central stencil entry, minus the sum of absolute values of all other entries. Using (10) and grouping all terms by the four diffusion tensor locations $(i \pm \frac{1}{2}, j \pm \frac{1}{2})$ gives

$$\begin{aligned} \rho(\mathbf{A}) \leq \frac{1}{2h^2} \max_{a,b,c} & \left(((a-\delta) + |a-\delta| + (\delta+b) + |\delta+b| + (c-\delta) + |c-\delta|)_{i-\frac{1}{2}, j-\frac{1}{2}} \right. \\ & + ((a-\delta) + |a-\delta| + (\delta-b) + |\delta-b| + (c-\delta) + |c-\delta|)_{i-\frac{1}{2}, j+\frac{1}{2}} \\ & + ((a-\delta) + |a-\delta| + (\delta-b) + |\delta-b| + (c-\delta) + |c-\delta|)_{i+\frac{1}{2}, j-\frac{1}{2}} \\ & \left. + ((a-\delta) + |a-\delta| + (\delta+b) + |\delta+b| + (c-\delta) + |c-\delta|)_{i+\frac{1}{2}, j+\frac{1}{2}} \right). \end{aligned} \quad (13)$$

Next, we bound the right hand side from above by assuming that the diffusion tensors at the different locations are independent. The notation

$$M_{\pm} := (a-\delta) + |a-\delta| + (\delta \pm b) + |\delta \pm b| + (c-\delta) + |c-\delta| \quad (14)$$

allows us to rewrite the bound as

$$\rho(\mathbf{A}) \leq \frac{1}{h^2} \left(\max_{a,b,c} (M_+) + \max_{a,b,c} (M_-) \right). \quad (15)$$

In the following, we determine the maximum of M_+ . Calculations for M_- are analogous. Notice that in M_+ , the three terms $a - \delta$, $\delta + b$, and $c - \delta$ appear

pairwise with their absolute values. This will simplify the calculation of the maximum. Consider the sum of the three terms:

$$m_+ := (a - \delta) + (\delta + b) + (c - \delta) = a + b + c - \delta. \quad (16)$$

If m_+ has a maximum in which $a - \delta$, $\delta + b$, and $c - \delta$ are all nonnegative, then $\max(M_+) = 2 \max(m_+)$, since $x + |x| = 2x$ for $x \geq 0$. We now proceed to show that such a maximum of m_+ exists. To this end, we rewrite the entries a , b , and c of the positive semidefinite diffusion tensor \mathbf{D} in terms of its normalised eigenvectors $(u, v)^\top$, $(v, -u)^\top$ and their eigenvalues $\lambda_1 \geq \lambda_2 \geq 0$:

$$a = \lambda_1 u^2 + \lambda_2 v^2, \quad b = (\lambda_1 - \lambda_2) uv, \quad c = \lambda_2 u^2 + \lambda_1 v^2. \quad (17)$$

The possible ranges for eigenvalues may differ between diffusion models. Therefore, we determine the maximum of m_+ , and by extension our limit on $\rho(\mathbf{A})$, as a function of λ_1 and λ_2 . This leaves the entries u, v of the eigenvectors as the only variables to maximise m_+ over. Using (17) in (16) gives

$$\begin{aligned} \max_{u,v} (m_+) &= \max_{u,v} ((1-\alpha)(\lambda_1 + \lambda_2) + (1-\beta)(\lambda_1 - \lambda_2) uv) \\ &= \max_{u,v} ((1-\alpha)(\lambda_1 + \lambda_2) + (1-\gamma(1-2\alpha) \operatorname{sgn}(uv)) (\lambda_1 - \lambda_2) uv) \\ &= \max_{u,v} \begin{cases} (1-\alpha)(\lambda_1 + \lambda_2) + \underbrace{(1-\gamma(1-2\alpha))}_{\geq 0} \underbrace{(\lambda_1 - \lambda_2)}_{\geq 0} \underbrace{uv}_{>0} & \text{for } uv > 0, \\ (1-\alpha)(\lambda_1 + \lambda_2) + \underbrace{(1+\gamma(1-2\alpha))}_{\geq 0} \underbrace{(\lambda_1 - \lambda_2)}_{\geq 0} \underbrace{uv}_{\leq 0} & \text{for } uv \leq 0. \end{cases} \end{aligned} \quad (18)$$

The case where $uv > 0$ gives always larger results than the second one. Thus,

$$\max_{u,v} (m_+) = \max_{u,v} ((1-\alpha)(\lambda_1 + \lambda_2) + (1-\gamma(1-2\alpha)) (\lambda_1 - \lambda_2) uv). \quad (19)$$

We maximise the second term by maximising uv . For our normalised eigenvectors, $u^2 + v^2 = 1$ holds. Hence, $\max(uv) = \frac{1}{2}$ for $u = v = \pm \frac{1}{\sqrt{2}}$. Since we only need the maximal function value, we can consider only $u = v = \frac{1}{\sqrt{2}}$. This gives

$$\max_{u,v} (m_+) = (1-\alpha)(\lambda_1 + \lambda_2) + \frac{1}{2} (1-\gamma(1-2\alpha)) (\lambda_1 - \lambda_2). \quad (20)$$

We are not able to draw conclusions about the maximum of M_+ from the maximum of m_+ yet. It remains to show that $a - \delta$, $\delta + b$, and $c - \delta$ are all nonnegative in our maximum with $u = v = \frac{1}{\sqrt{2}}$. We start with $a - \delta$ and use (17):

$$\begin{aligned} (a - \delta)|_{u=v=\frac{1}{\sqrt{2}}} &= (a - \beta b - \alpha(a + c))|_{u=v=\frac{1}{\sqrt{2}}} \\ &= \frac{1}{2} ((\lambda_1 + \lambda_2) - \gamma \underbrace{(1-2\alpha)}_{\geq 0} \underbrace{(\lambda_1 - \lambda_2)}_{\geq 0} - 2\alpha(\lambda_1 + \lambda_2)) \\ &\geq \frac{1}{2} ((\lambda_1 + \lambda_2) - (1-2\alpha)(\lambda_1 - \lambda_2) - 2\alpha(\lambda_1 + \lambda_2)) \\ &= (1-2\alpha)\lambda_2 \geq 0. \end{aligned} \quad (21)$$

In a similar way, one shows $(c - \delta)|_{u=v=\frac{1}{\sqrt{2}}} \geq 0$. For $b + \delta$ we verify

$$\begin{aligned} (b + \delta)|_{u=v=\frac{1}{\sqrt{2}}} &= ((1 + \beta)b + \alpha(a + c))|_{u=v=\frac{1}{\sqrt{2}}} \\ &= \frac{1}{2} \underbrace{(1 + \gamma(1 - 2\alpha))}_{\geq 0} \underbrace{(\lambda_1 - \lambda_2)}_{\geq 0} + \alpha(\lambda_1 + \lambda_2) \geq 0. \end{aligned} \quad (22)$$

As all three terms are nonnegative in the maximum, we can conclude that

$$\max_{u,v}(M_+) = 2 \max_{u,v}(m_+) = 2(1 - \alpha)(\lambda_1 + \lambda_2) + (1 - \gamma(1 - 2\alpha))(\lambda_1 - \lambda_2). \quad (23)$$

Analogous computations lead to the same maximum for M_- . Inserting both into (15) produces the claimed bound on the spectral norm. \square

Using Theorem 1 within (11) directly gives the following time step size limit:

Corollary 1 (Stability of Explicit Scheme). *An explicit anisotropic diffusion scheme $\mathbf{u}^{k+1} = (\mathbf{I} + \tau \mathbf{A}(\mathbf{u}^k)) \mathbf{u}^k$, where \mathbf{A} satisfies the assumptions of Theorem 1 with $\lambda_1 > 0$, is stable in the Euclidean norm for*

$$\tau \leq \frac{h^2}{2(1 - \alpha)(\lambda_1 + \lambda_2) + (1 - \gamma(1 - 2\alpha))(\lambda_1 - \lambda_2)}. \quad (24)$$

While our proof does not guarantee that this bound is strict, our practical experience suggests that it is. Corollary 1 covers two important special cases:

1. In the **homogeneous diffusion case** with $\lambda_1 = \lambda_2 = 1$, this time step size limit simplifies to $\tau \leq \frac{h^2}{4(1 - \alpha)}$. Moreover, setting $\alpha := 0$ turns the δ -stencil into the standard five point approximation of the Laplacian, which leads to the well-known 2-D time step size limit $\tau \leq \frac{h^2}{4}$; see e.g. [5].
2. In the **maximally anisotropic case** with $\lambda_1 = 1$, $\lambda_2 = 0$, and $\gamma = 1$, one performs 1-D diffusion along one eigendirection of \mathbf{D} . Then (24) becomes $\tau \leq \frac{h^2}{2}$. In spite of being in a 2-D setting, this coincides with the typical 1-D time step size limit [5], which is less restrictive. This shows that our scheme takes full advantage of the anisotropy. In image analysis, this result is relevant for coherence-enhancing nonlinear diffusion filters [11]. Similar findings have also been made with a recent numerical scheme for a maximally anisotropic backward parabolic PDE [10].

4 Translating Anisotropic Diffusion into ResNets

Let us now interpret our explicit scheme in the context of neural networks. This extends the result of Alt et al. [1] from the 1-D setting to the 2-D anisotropic case. We start by presenting their translation of 1-D diffusion into a ResNet block, and then build the anisotropic ResNet block from there.

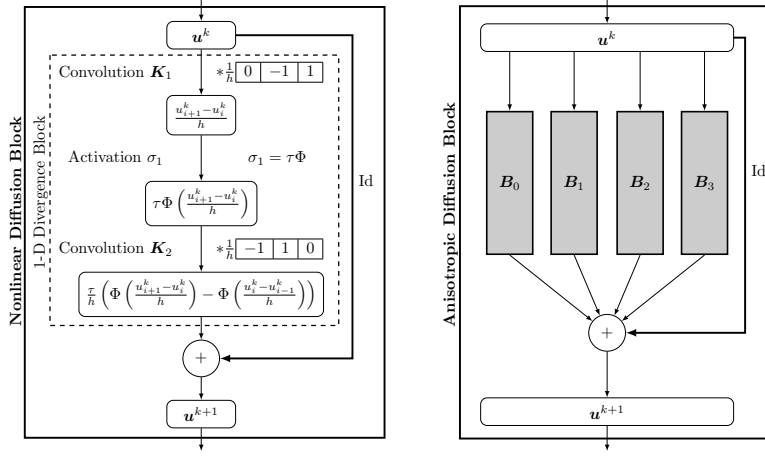


Fig. 1. (a) **Left:** Translation of 1-D nonlinear diffusion into a ResNet block. Adapted from [1]. (b) **Right:** Anisotropic diffusion as a ResNet block with a sum of four 1-D divergence blocks. The blocks B_0, \dots, B_3 correspond to the directions $\mathbf{e}_0, \dots, \mathbf{e}_3$.

ResNets. Residual networks (ResNets) [4] are very popular neural network architectures. They use ResNet blocks that compute an output \mathbf{u}^{k+1} from an input \mathbf{u}^k by

$$\mathbf{u}^{k+1} = \sigma_2(\mathbf{u}^k + \mathbf{K}_2 \sigma_1(\mathbf{K}_1 \mathbf{u}^k + \mathbf{b}_1) + \mathbf{b}_2) \quad (25)$$

for discrete convolution kernels $\mathbf{K}_1, \mathbf{K}_2$, bias vectors $\mathbf{b}_1, \mathbf{b}_2$, and nonlinear activation functions σ_1, σ_2 such as the ReLU function $\sigma(x) = \max\{x, 0\}$. Adding the input \mathbf{u}^k before applying the second activation σ_2 helps to avoid vanishing gradients and to improve stability. This allows to train very deep networks.

Translating 1-D Diffusion into ResNets. The basic translation of 1-D diffusion into ResNets is surprisingly simple [1,9]: In vector notation, the explicit scheme (3) becomes

$$\mathbf{u}^{k+1} = \mathbf{u}^k + \tau \mathbf{D}_h^- (\Phi(\mathbf{D}_h^+ \mathbf{u}^k)). \quad (26)$$

Here, \mathbf{D}_h^+ and \mathbf{D}_h^- represent matrices computing forward and backward first order derivative approximations with grid size h . Comparing (26) to the ResNet block (25) reveals that both perform the same computations when identifying

$$\mathbf{K}_1 = \mathbf{D}_h^+, \quad \sigma_1 = \tau \Phi, \quad \mathbf{K}_2 = \mathbf{D}_h^-, \quad \mathbf{b}_1 = \mathbf{b}_2 = \mathbf{0}, \quad \sigma_2 = \text{Id}. \quad (27)$$

The computational graph for this is shown in Figure 1(a).

Alt et al. [1] use this connection to advocate ResNet architectures with mirrored kernels \mathbf{K}_1 and \mathbf{K}_2 to guarantee stability in the Euclidean norm. Moreover, their experiments show advantages of nonmonotone activation functions.

Translating 2-D Anisotropic Diffusion into ResNets. Our directional splitting allows also a natural translation of anisotropic diffusion into ResNets.

We split the divergence term of 2-D anisotropic diffusion into a sum of four divergence terms of 1-D diffusion processes, and use the previous translation for each. This is illustrated in Figure 1(b). By appropriately concatenating the 2-D convolution kernels into 4-D tensors, we match the ResNet structure precisely.

Experiments. Implementing numerical schemes for GPUs using CUDA can be labour-intensive and requires expertise. However, deep learning frameworks are capable of fully automatic and efficient parallelisation of user code. As we were able to decompose our discretisation into neural network primitives, we can use these frameworks to obtain an efficient implementation with little effort.

We consider 10 iterations of an explicit scheme for edge-enhancing image diffusion (EED) [11] and compare three implementations. The first uses C and runs on the CPU. It computes entries of the δ -stencil before applying it to the image. The second is an implementation in the PyTorch framework which follows the same strategy. As this style is uncommon in most neural networks, the implementation is fairly involved. The third also uses PyTorch, but follows our ResNet translation. It only requires two convolutions, one activation function, and a summation. This leads to a concise and simple implementation.

For an image with 2048×2048 pixels, our C code takes 1.6 s on an AMD 5800X CPU. Both PyTorch implementations perform one order of magnitude faster at 0.16 s and 0.15 s respectively on an Nvidia 3090 GPU. This demonstrates that our ResNet translation is able to significantly accelerate EED with a straightforward parallel implementation. It is even as fast as the much more involved stencil-based GPU implementation. This behaviour is consistent across image and batch sizes, provided that the total pixel count is sufficiently large.

5 Conclusions

We have explored three aspects of anisotropic diffusion stencils. The first was an intuitive derivation of a large second-order stencil family based on directional splitting. While it covers the full stencil class of Weickert et al. [13], its derivation is simpler, and it requires only one free parameter (δ) instead of two. Therefore, we call it the δ -stencil family.

Secondly, we have established a rigorous spectral norm estimate of the matrix associated to this stencil family. It allows to derive fairly tight time step size limits of explicit schemes to guarantee stability in the Euclidean norm. We have restricted ourselves to explicit schemes, since they are structurally similar to feedforward neural networks. Moreover, they form the backbone of acceleration methods based on super time stepping [12] and extrapolation concepts [3]. Further multigrid-like acceleration options may arise from multiscale network features such as pooling operations and U-net structures [1].

Thirdly, the directional splitting from our derivation has been instrumental in linking anisotropic diffusion to ResNets. It paves the road to an effortless and efficient parallelisation with libraries such as PyTorch. This also illustrates the usefulness of neural networks outside their original field of machine learning.

In our ongoing work, we also address the reverse direction: We investigate how neural architectures can benefit from the integration of anisotropic diffusion.

Acknowledgements. We thank Kristina Schaefer for careful proofreading.

References

1. Alt, T., Schrader, K., Augustin, M., Peter, P., Weickert, J.: Connections between numerical algorithms for PDEs and neural networks. *Journal of Mathematical Imaging and Vision* 65, 185–208 (Jan 2023)
2. Alt, T., Schrader, K., Weickert, J., Peter, P., Augustin, M.: Designing rotationally invariant neural networks from PDEs and variational methods. *Research in the Mathematical Sciences* 9(3), Article 52 (Sep 2022)
3. Hafner, D., Ochs, P., Weickert, J., Reißel, M., Grewenig, S.: FSI schemes: Fast semi-iterative solvers for PDEs and optimisation methods. In: Rosenhahn, B., Andres, B. (eds.) *Pattern Recognition, Lecture Notes in Computer Science*, vol. 9796, pp. 91–102. Springer, Cham (2016)
4. He, K., Zhang, X., Ren, S., Sun, J.: Deep residual learning for image recognition. In: *Proc. 2016 IEEE Conference on Computer Vision and Pattern Recognition*. pp. 770–778. Las Vegas, NV (Jun 2016)
5. Morton, K.W., Mayers, L.M.: *Numerical Solution of Partial Differential Equations*. Cambridge University Press, Cambridge, UK, second edn. (2005)
6. Mrázek, P., Navara, M.: Consistent positive directional splitting of anisotropic diffusion. In: Likar, B. (ed.) *Proc. Sixth Computer Vision Winter Workshop*. pp. 37–48. Bled, Slovenia (Feb 2001)
7. Perona, P., Malik, J.: Scale space and edge detection using anisotropic diffusion. *IEEE Transactions on Pattern Analysis and Machine Intelligence* 12, 629–639 (Jul 1990)
8. Rousseau, F., Drumetz, L., Fablet, R.: Residual networks as flows of diffeomorphisms. *Journal of Mathematical Imaging and Vision* 62, 365–375 (Apr 2020)
9. Ruthotto, L., Haber, E.: Deep neural networks motivated by partial differential equations. *Journal of Mathematical Imaging and Vision* 62, 352–364 (Apr 2020)
10. Schaefer, K., Weickert, J.: Stabilised inverse flowline evolution for anisotropic image sharpening. In: *Proc. 10th European Workshop on Visual Information Processing*. Lisbon, Portugal (Sep 2022)
11. Weickert, J.: *Anisotropic Diffusion in Image Processing*. Teubner, Stuttgart (1998)
12. Weickert, J., Grewenig, S., Schroers, C., Bruhn, A.: Cyclic schemes for PDE-based image analysis. *International Journal of Computer Vision* 118(3), 275–299 (Jul 2016)
13. Weickert, J., Welk, M., Wickert, M.: L^2 -stable nonstandard finite differences for anisotropic diffusion. In: Kuijper, A., Bredies, K., Pock, T., Bischof, H. (eds.) *Scale Space and Variational Methods in Computer Vision, Lecture Notes in Computer Science*, vol. 7893, pp. 390–391. Springer, Berlin (2013)
14. Welk, M.: Diffusion, pre-smoothing and gradient descent. In: Elmoataz, A., Fadili, J., Quéau, Y., Rabin, J., Simon, L. (eds.) *Scale Space and Variational Methods in Computer Vision, Lecture Notes in Computer Science*, vol. 12679, pp. 78–90. Springer, Cham (2021)
15. Wendland, H.: *Numerical Linear Algebra: An Introduction*. Cambridge University Press, Cambridge, UK (2018)